

Analysis of *Fermi*-LAT data from Tucana-II: Possible constraints on the Dark Matter models with an intriguing hint of a signal

Pooja Bhattacharjee^{1,2,*}, Sayan Biswas^{3,†}, Pratik Majumdar^{4,‡} and Partha S. Joarder^{1,2§}

¹ Department of Physics, Bose Institute, 93/1 A.P.C. Road, Kolkata 700009, India

² Centre for Astroparticle Physics and Space Science, Bose Institute,

Block EN, Sector V, Salt Lake, Kolkata 700091, India

³ Raman Research Institute, C.V. Raman Avenue, Sadashivanagar, Bangalore 560080, India and

⁴ Saha Institute of Nuclear Physics, HBNI, 1/AF, Bidhannagar, Kolkata 700064, India

Tucana-II (Tuc-II), a recently discovered and confirmed Ultra Faint Dwarf Spheroidal galaxy, has a high mass to light ratio as well as a large line-of-sight stellar velocity dispersion, thus making it an ideal candidate for an indirect dark matter (DM) search. In this paper, we have analyzed nine years of γ -ray data obtained from the *Fermi*-LAT instrument from the direction of Tuc-II. The fact that a very weak significant γ -ray excess ($\sim 2.9\sigma$) over the background of Tuc-II have been detected from the location of this galaxy. We have observed that this excess of γ -ray emission from the location of Tuc-II rises with longer periods of data. If WIMP pair annihilation is assumed for this faint emission, for $b\bar{b}$ annihilation channel the test statistics (TS) value peaks at DM mass ~ 14 GeV and for $\tau^+\tau^-$ annihilation channel it peaks at DM mass ~ 4 GeV. It is then called for an estimation of the 95% confidence level upper limit of the possible velocity weighted self-annihilation cross-section of the DM particles (WIMPs) within Tuc-II by fitting the observed γ -ray flux with spectra expected for DM annihilation. The estimated upper limits of the cross-sections from Tuc-II are then compared with two other dwarf galaxies that are considered to be good DM candidates in several studies. We have also compared our results with the cross-sections obtained in various popular theoretical models of the WIMPs to find that our results impose reasonable tight constraints on the parameter spaces of those DM models. In the concluding section, we compared our results with the similar results obtained from a combined dSph analysis by the *Fermi*-LAT collaboration as well as the results obtained from the studies of DM in the dwarf galaxies by the major ground-based Cherenkov experiments.

Keywords: dark matter, WIMP, ultra faint dwarf spheroidal galaxy, indirect detection.

1. INTRODUCTION

The astrophysical and cosmological observations (e.g. [1, 2]) strongly suggest that some kind of non-luminous and non-baryonic matter, namely the Dark Matter (DM), constitutes almost 75% of the total matter density of the Universe. Regarding the physical nature of such DM, cosmological N-body simulations (e.g. [3, 4]) usually, favor a cold DM (CDM) scenario to explain the formation of the large scale structure of the Universe. In addition, the extension of the Standard Model (SM) of particle physics predicts that CDM could possibly consist of some form of massive, non-baryonic and neutrally charged particles, namely weakly interacting massive particles (WIMPs). WIMPs self pair annihilation (with their masses lying in the range of a few tens of GeV to a few hundreds of TeV) explains the thermal relic abundances (i.e. $\langle \sigma v \rangle \approx 3 \times 10^{-26} \text{ cm}^3 \text{ s}^{-1}$) and are consistent with the currently observed mass density of CDM; e.g.. [5–7]. Such pair-annihilation of the WIMPs may be one of the excellent source of indirect dark matter search [5].

DM pair-annihilation rate and the resulting flux of γ -photons are likely to be proportional to the square of the DM density. The dwarf Spheroidal satellite galaxies (dSph) of the Milky Way (MW) that are the densest DM regions in the galactic halo [8], usually lie away from the direction of the central region of the galaxy. Those dSphs are not too far ($\sim (20 - 200)$ kpc) from the earth [9] and they have low content of gas and dust [10], therefore, making them the potentially excellent targets for an indirect search of DM through the detection of the high energy γ -rays arising from the WIMP annihilations [5, 11, 12]. Over about a decade from now, the Sloan Digital Sky Survey

*pooja.bhattacharjee@jcbose.ac.in

†sayan@rrri.res.in

‡pratik.majumdar@saha.ac.in

§partha@jcbose.ac.in

(SDSS) [13, 14], the Panoramic Survey Telescope and Rapid Response System (Pan-STARRS) [15–17], the Dark Energy Survey (DES) [18–21] experiment and certain other surveys by using the Dark Energy Camera at Cerro Tololo [22, 23] have discovered a new class of dSphs, namely the Ultra Faint Dwarf galaxies (UFDs) that have extremely low stellar contents and densities. The UFDs are dominated by old ($\gtrsim 12$ Gyr) stellar populations with large velocity dispersions that possibly indicate the existence of substantial DM components in those UFDs [24]. The recent N-body simulations also indicate the existence of a huge number of DM sub-halos around the MW’s halo[25, 26] and amongst them, few hundreds of these sub-halos might be massive enough to host a dwarf galaxy [25]. Thus, studying these old and metal-poor UFDs provide us a deep understanding on the nature of the ancient galaxies [27, 28] that were accreted to form the Milky Way halo [29, 30] and the origin of the chemical abundances of the stellar population of Milky Way halo[31]. Hence, with inferred mass-to-light ratios reaching up to $\sim 3000 M_\odot/L_\odot$, the UFDs are, therefore, considered to be the best tracers of early DM sub-halos in the Universe as predicted by the Λ CDM cosmological models [25, 26, 30, 32]. Recently, a joint DES-*Fermi* collaboration [33] has examined the γ -ray signatures of the WIMP pair-annihilations from about 45 UFDs. The aim of their study was to re-examine the constraints imposed on various theoretical WIMP models by an earlier analysis [5, 34–36] of the γ -ray data from 15 confirmed dSphs performed by the *Fermi* collaboration. At present, two new sky survey programs, namely the Large Synoptic Survey Telescope (LSST) and the Wide-Field Infrared Survey Telescope, are being undertaken/planned to search for more UFD/dSph candidates in the galactic halo and in its neighborhood for a comprehensive study of the DM in the Universe [37].

Motivated by such increasing interest in the indirect search for DM in the UFDs/dSphs, in the present paper, we focus our attention to a recently discovered dwarf satellite, namely Tucana-II (Tuc-II; DES J2251.2-5836) [19, 20, 38]. Tuc-II has already been confirmed to be a UFD (and not a part of any globular cluster) in Ref. [39], principally because of its large projected half light radius, the large velocity dispersion of its member stars, its luminosity-metallicity relation and also because of its large dynamical mass to light ratio, all of which conform to the well-established values of the dwarf galaxies [28, 39–42]. Tuc-II may, as well, be a member of the Magellanic group as it is only about 19 kpc away from the Large Magellanic Cloud (LMC) and about 37 kpc away from the Small Magellanic Cloud (SMC) [19]. The outer region of Tuc-II appears to be in an elongated and distorted shape but the observational noise could, as well, be the reason for such a distortion [19, 43, 44]. Considering various observationally inferred parameter values of Tuc-II, Walker *et al.*, 2016 [39] had suggested that this UFD may not exhibit one of the strongest DM annihilation signal, but may contribute meaningfully to the analysis of stacked data from multiple sources including Tuc-II. Many groups have already studied the Tuc-II in search of dark matter self-annihilation [33, 45–47].

In this paper, we performed a data analysis of Tuc II with 9 years of *Fermi*-LAT data to search the dark matter signal. We observed a faint emission from the direction of Tuc-II for two WIMP pair annihilation channels and we showed the significant increment of the test statistic (TS) peak values from the direction of Tuc-II with larger periods of data. Both the test statistic (TS) and the statistical significance (i.e., the p -value) of the best-fitted spectra for this excess emission, apparently favors a DM annihilation spectra over a simple power-law spectra, that seems to undermine an astrophysical origin of the emission. The residual TS map around Tuc-II, generated in this paper, seems to suggest that the excess signal is localized at the position of Tuc-II, apparently ruling out the possibility that, the faint excess may be due to some unrelated background sources or simply due to the random fluctuation in the ‘local background’ around Tuc-II. Admittedly, the significance of the excess emission in the direction of Tuc-II, obtained in this paper, is much weaker than the threshold of the *Fermi*-LAT’s detection but it gives a hint of dark matter signal. Such emission from Tuc-II location has not been reported before by any other groups. Moreover, we calculated the possible upper limits of the velocity-averaged pair-annihilation cross-section $\langle \sigma v \rangle$ of the WIMPs from Tuc-II and compared with the ones obtained from the analysis of Ursa Minor (UMi). Later, we also compared our results with the ones obtained from the recent DES-discovered UFD, namely Reticulum-II (Ret-II) [19, 20, 48–50]. The *Fermi*-LAT data analysis of Ret-II has already been done in Refs. [33, 45, 47, 51–53] and that seems to exhibit a small excess of γ -ray signal of some significance over the background of Ret-II, thus making Ret-II an attractive source to search for the annihilation signals of DM. Our comparison, presented in this paper, showed that the constraints imposed by Tuc-II on the popular WIMP models for $b\bar{b}$ annihilation channel are comparable to the ones expected in the case of Ret-II. Furthermore, with nine years of *Fermi*-LAT data, we have compared the resulting LAT sensitivity for Tuc-II with predictions obtained from four theoretical models. For the sake of such study, we here assume a perfect spherical symmetry for Tuc-II and further assume Tuc-II to be in dynamic equilibrium with a negligible contribution to its significantly large, observed line-of-sight stellar velocity dispersion from the possible binary stellar motions in Tuc-II, thus assuming that the gravitational potential of Tuc-II is entirely dominated by DM [39].

The paper is organized along the following line. After stating the observed properties of Tuc-II (in subsection 2.1)

that are relevant for our study, we briefly describe the procedure for the analysis of *Fermi*-LAT data from the direction of Tuc-II in subsection 2.2. In subsection 2.3, we estimate the upper limits of the γ -ray flux from Tuc-II by fitting Tuc-II with power-law spectral model with five different power indices. In subsection 3.1, we employ the NFW density profile to model the DM density in UFDs. In that subsection, we also estimate the J-factor and its uncertainties for the possible γ -ray flux arising from the WIMP pair-annihilation in UFDs. In subsection 3.2, we first report a faint γ -ray emission ($\sim 2.9\sigma$) from Tuc-II possibly resulting from WIMP pair annihilation to $\tau^+\tau^-$ channel by using the DMfit Monte Carlo (MC) simulation package [54] and study the nature of this excess emission for three, six and nine years of *Fermi*-LAT data. Then we have studied the distribution of excess obtained from the location of Tuc-II and the possible reason responsible for such faint emission. Next we determine the possible upper limit of the γ -ray flux from Tuc-II. There, we also calculate the possible upper limits of the velocity-averaged pair-annihilation cross-section $\langle \sigma v \rangle$ of the WIMPs for several important pair-annihilation channels and compare those cross-sections with the ones obtained from various theoretical WIMP models in section 3.2. Comparisons of the $\langle \sigma v \rangle$ upper limit from Tuc-II, with the results obtained from Ret-II and UMi, are also presented in subsection 3.2 of this paper. Finally, a brief discussion of our results presented here *vis-a-vis* the results obtained from UFDs/dSphs with the *Fermi*-LAT and with various ground-based Cherenkov experiments at higher energies are presented in the concluding section 4.

2. ANALYSIS OF TUC-II

2.1. The relevant observed properties of Tuc-II

A spectroscopic study of a number of stars in the direction of Tuc II was undertaken by Walker *et al.*, 2016 [39] by the use of the Michigan Magellan Fibre System (M2FS). This study [39], along with the previous photometric results on Tuc-II [20, 38], could identify eight probable member stars of Tuc-II that were sufficiently well-resolved to determine an internal velocity dispersion but with large asymmetrical uncertainties, $\sigma_v = 8.6_{-2.7}^{+4.4} \text{ km s}^{-1}$ about a mean velocity of $-129.1_{-3.5}^{+3.5} \text{ km s}^{-1}$ in the solar rest frame. These and the other important physical properties of Tuc-II that have either been directly observed or have been inferred from the observations of Tuc-II by the authors of Refs. [20, 39, 55], are tabulated in TABLE 1 for later reference.

TABLE 1: Properties of Tuc-II

| Property | Value | Reference |
|--|--|-----------|
| Galactic longitude | 328.0863° | [20] |
| Galactic latitude | -52.3248° | [20] |
| Heliocentric distance ([d]) | 57_{-5}^{+5} kpc | [20] |
| Metallicity ([Fe/H]) | < 0.4 | [39] |
| Projected half light radius (R_h) | $165_{-18.5}^{+27.8} \text{ pc}$ | [20] |
| Maximum galactocentric angular distance in the sample of the observed member stars in Tuc-II, as measured from the observer's position ($[\theta_{\max}]$) | 0.30° | [55] |
| Square-root of the luminosity-weighted square of the line-of-sight stellar velocity dispersion (σ_v) | $8.6_{-2.7}^{+4.4} \text{ km s}^{-1}$ | [39] |
| Mass within the projected half-light radius ($\frac{M_{1/2}}{M_\odot}$) | $2.7_{-1.3}^{+3.1} \times 10^6$ | [39] |
| Dynamical mass-to-light ratio ($(M/L_v)_{1/2}$) | $1913_{-950}^{+2234} M_\odot L_\odot^{-1}$ | [39] |

In TABLE 1, M_{\odot} and L_{\odot} indicate the mass and the total luminosity of the Sun, respectively. Definitions of various other quantities displayed in TABLE 1 are given in [20, 39, 55]; also see Refs.[56–58]. In the subsection 3.1, we will use some of the parameters of Tuc-II enlisted in TABLE 1 to evaluate the so-called J-factor, and hence the γ -ray flux arising from DM annihilation in Tuc-II.

2.2. The *Fermi*-LAT data analysis of Tuc-II

The *Fermi*-LAT is a γ -ray space-based detector that scans the whole sky every 3 hour for an efficient study of the γ -ray sky in an energy range from about 20 MeV to 500 GeV. In this paper, we have used the recent version v10r0p5 of the *Fermi* ScienceTools for the analysis of γ -ray data from Tuc-II. The above version allows us to use the pre-processed PASS 8 dataset of event class 128 that makes use of an improved instrument response function (IRF) P8R2_SOURCE_V6 of the LAT.

We have extracted nearly nine years (i.e. from 2008-05-04 to 2017-10-22) of LAT data in 100 MeV to 300 GeV reconstructed energy range within a $10^{\circ} \times 10^{\circ}$ radius of interest (ROI) centered on the location of Tuc-II. In the source model, we have included Tuc-II along with all the point sources from 3FGL catalog within 15° of ROI from the position of Tuc-II. We have then performed the binned likelihood analysis on our extracted dataset with the ‘gtlike’ tool [59, 60] by following the instructions given in the *ScienceTools*. The spectral parameters of all the *Fermi*-3FGL sources [61] within ROI, as well as, the normalization parameters of two diffuse models (i.e. gll_iem_v06.fits and iso_P8R2_SOURCE_V6_v06.txt) have been left free during the model fitting procedure. The rest of all the background sources within the $15^{\circ} \times 15^{\circ}$ ROI have been kept fixed at their values given in the 3FGL catalog [61]. All the required information related to our *Fermi*-LAT analysis method is mentioned in TABLE 2.

In the following, we first model Tuc-II as a source having a power-law spectrum with each of the five different spectral indices and later in section 3.2, we go over to fit the γ -ray spectrum arising from the (assumed) DM-dominated Tuc-II with an MC-simulated DM self-annihilation spectrum generated by the use of the DMFit simulation tool-kit [54].

2.3. Results of the power-law modeling

The form of the differential photon flux for power-law modeling can be expressed as:

$$\frac{dN}{dAdEdt} = N_0 \left(\frac{E}{E_0} \right)^{-\Gamma}, \quad (1)$$

where, dN denotes the number of photons lying between the energy range of E and $E + dE$. dA is the elemental area of detector, in which, photons are incident in time interval, dt .

From Eq. (1) N_0 and Γ define the normalization parameter and the spectral index of power-law modeling, respectively, while, E denotes the reconstructed energy. For our analysis we have set the energy scale (E_0) at 100 MeV [5] and dE is varied from 100 MeV to 300 GeV.

In Fig. 1(a), we display the spectral fit per energy bin of all the sources within the aforesaid ROI, along with the isotropic background component and the galactic diffuse background component. Similarly, Fig. 1(b) displays the corresponding residual plot for all the above sources in the given ROI. The horizontal axes in both these figures indicate the reconstructed energy E of the γ -photons within the chosen range. While the above figures display only the results for modeling Tuc-II with a spectral index $\Gamma = 2$ alone, we have actually repeated this spectral fitting procedure for each of the other values of the spectral index, namely $\Gamma = 1, 1.8, 2.2$ and 2.4 , as well.

The best-fitted values of the N_0 and the TS obtained from Tuc-II for each of those spectral indices (Γ) are displayed in TABLE 3. The TS value is the ratio of the maximum likelihoods for two hypothesis, in which, $L_{(\max,1)}$ denotes the maximum likelihood for full model and $L_{(\max,0)}$ refers to the maximum likelihood for the null hypothesis. The expression of TS value is $TS = -2 \ln \left(L_{(\max,0)} / L_{(\max,1)} \right)$. Among those aforementioned spectral indices, $\Gamma = 1$ is preferred for its connection with the DM annihilation models in Ref. [62] and the other four Γ ’s are chosen to examine the general astrophysical source spectrum. In TABLE 3, for $\Gamma = 1$, the error on N_0 is slightly higher than the value N_0 itself and it denotes the no-significance from the direction of Tuc-II and the TS values for other Γ s are

TABLE 2: Parameters used in Science Tools for *Fermi*-LAT data analysis

| Parameter for data extraction ^a | |
|---|---|
| Parameter | Value |
| Source | Tucana-II |
| Right Ascension (RA) | 342.9796 |
| Declination (DEC) | -58.5689 |
| Radius of interest (ROI) | 10° |
| TSTART (MET) | 239557418 (2008-08-04 15:43:37.000 UTC) |
| TSTOP (MET) | 530362359 (2017-10-22 10:52:34.000 UTC) |
| Energy Range | 100 MeV - 300 GeV |
| <i>Fermi</i> -LAT Science Tool version | v10r0p5 ^b |
| gtselect for event selection ^c | |
| Event class | Source type (128) ^d |
| Event type | Front+Back (3) ^d |
| Maximum zenith angle cut | 90° ^d |
| gtmktime for time selection ^e | |
| Filter applied | (DATA_QUAL > 0)&&(LAT_CONFIG == 1) ^f |
| ROI-based zenith angle cut | No ^f |
| gtltcube for livetime cube ^g | |
| Maximum zenith angle cut (z_{cut}) | 90° ^h |
| Step size in $\cos(\theta)$ | 0.025 |
| Pixel size (degrees) | 1 |
| gtbin for 3-D (binned) counts map ⁱ | |
| Size of the X & Y axis (pixels) | 140 |
| Image scale (degrees/pixel) | 0.1 |
| Coordinate system | Celestial (CEL) |
| Projection method | AIT |
| Number of logarithmically uniform energy bins | 24 |
| gtexpcube2 for exposure map ^j | |
| Instrument Response Function (IRF) | P8R2_SOURCE_V6 ^k |
| Size of the X & Y axis (pixels) | 400 |
| Image scale (degrees/pixel) | 0.1 |
| Coordinate system | Celestial (CEL) |
| Projection method | AIT |
| Number of logarithmically uniform energy bins | 24 |
| diffuse models and Source model XML file ^l | |
| Galactic diffuse emission model | gll_iem_v06.fits ^m |
| Extragalactic isotropic diffuse emission model | iso_P8R2_SOURCE_V6_v06.txt ^m |
| Source catalog | 3FGL |
| Extra radius of interest | 5° |
| Spectral model of Tucana-II | Power law (in Section-2.3) & DMFit Function (in Section-3.2) ⁿ |
| gtlike for likelihood analysis ^o | |
| Response functions | P8R2_SOURCE_V6 ^k |
| Optimizer | NEWMINUIT |

^ahttps://fermi.gsfc.nasa.gov/ssc/data/analysis/scitools/extract_latdata.html^b<https://fermi.gsfc.nasa.gov/ssc/data/analysis/software/>^c<https://fermi.gsfc.nasa.gov/ssc/data/analysis/scitools/help/gtselect.txt>^dhttps://fermi.gsfc.nasa.gov/ssc/data/analysis/documentation/Cicerone/Cicerone_Data_Exploration/Data_preparation.html^e<https://fermi.gsfc.nasa.gov/ssc/data/analysis/scitools/help/gtmktime.txt>^fhttps://fermi.gsfc.nasa.gov/ssc/data/analysis/scitools/data_preparation.html^g<https://fermi.gsfc.nasa.gov/ssc/data/analysis/scitools/help/gtltcube.txt>^hhttps://fermi.gsfc.nasa.gov/ssc/data/analysis/documentation/Cicerone/Cicerone_Likelihood/Exposure.htmlⁱ<https://fermi.gsfc.nasa.gov/ssc/data/analysis/scitools/help/gtbin.txt>^j<https://fermi.gsfc.nasa.gov/ssc/data/analysis/scitools/help/gtexpcube2.txt>^khttps://fermi.gsfc.nasa.gov/ssc/data/analysis/documentation/Pass8_usage.html^l<https://fermi.gsfc.nasa.gov/ssc/data/analysis/user/make3FGLxml.py>^m<https://fermi.gsfc.nasa.gov/ssc/data/access/lat/BackgroundModels.html>ⁿhttps://fermi.gsfc.nasa.gov/ssc/data/analysis/scitools/source_models.html^ohttps://fermi.gsfc.nasa.gov/ssc/data/analysis/scitools/binned_likelihood_tutorial.html

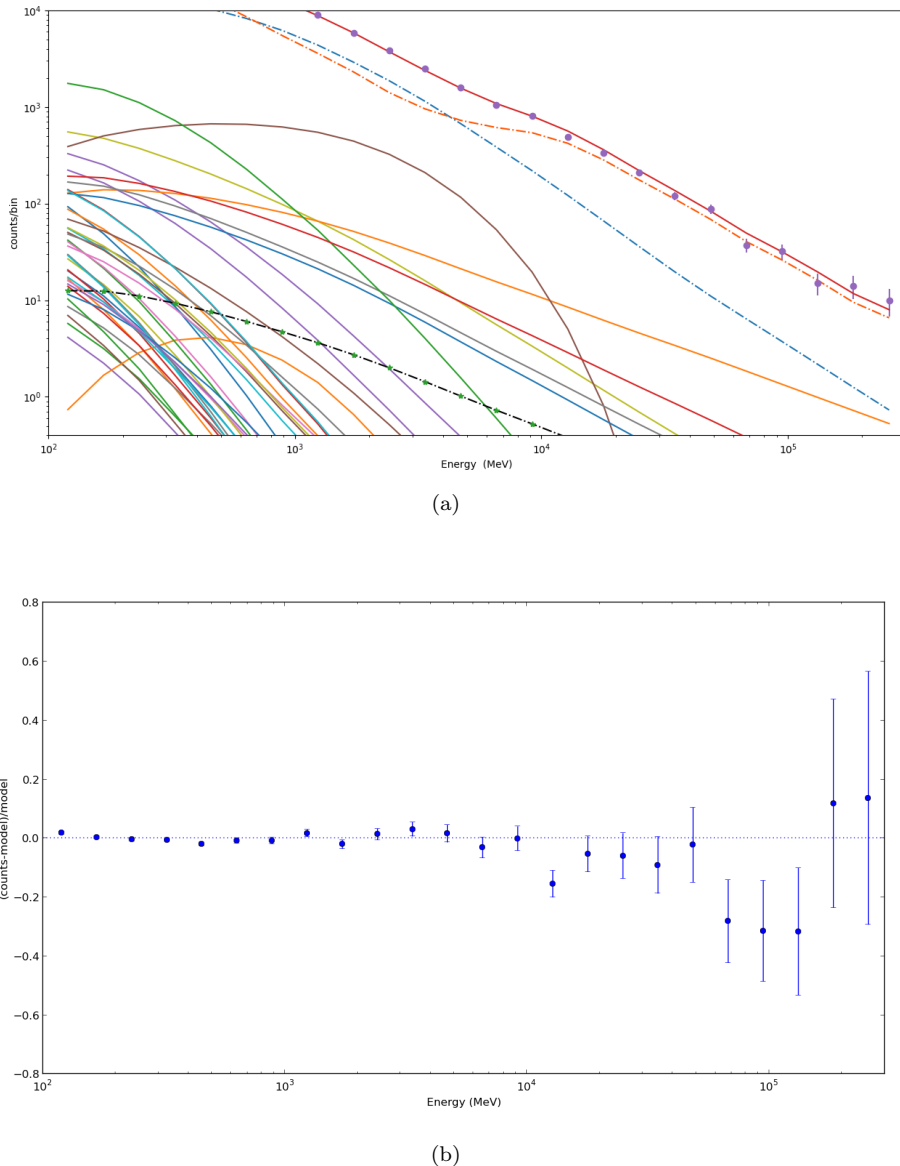


FIG. 1: Spectral fit to the counts per energy bin (Fig. 1(a)) and the corresponding residual plot (Fig. 1(b)) are displayed for all the sources within the chosen ROI centered on Tuc-II, in which the power-law source-spectral index of Tuc-II is taken as $\Gamma = 2$. In Fig. 1(a), the solid dark reddish-brown curve displays the best-fit total spectrum, along with the corresponding LAT-observed data points (in purple); the dot-dashed sky and orange curves display the galactic diffuse background and the isotropic background component, respectively; the dot-dashed black curve along with green points denotes the spectral fit of Tuc-II. The rest of the curves correspond to various point sources other than Tuc-II, lying within the ROI that are not distinctly labeled in Fig. 1(a).

also much less than the threshold-detection limit of *Fermi*-LAT (i.e. $TS \geq 25$).

Hence, we calculate the flux upper limit from Tuc-II over the entire reconstructed energy range ($0.1 - 300$) GeV by the profile likelihood method [63, 64]. During the process of estimating the flux upper limits, all the normalization parameters along with two diffuse components are fitted continuously with the entire dataset until the logarithmic difference of two likelihood functions arrives at the value of 1.35 [5] which corresponds to a one-sided 95% C.L.

As no significant excess is observed at the location of Tuc-II, we have next estimated the 95% flux upper limits by using the semi-Bayesian method with flat prior. For very low data statistics system, the semi-Bayesian method is generally favored over likelihood profile [63]. This Bayesian method is developed from Helene's approach [65]

TABLE 3: Best-fitted normalization parameters (N_0) and the TS values obtained from the spectral fittings of the γ -ray flux from Tuc-II with five different spectral indices (Γ).

| Spectral Index (Γ) | $N_0 \times 10^{-5}$ (cm $^{-2}$ s $^{-1}$ MeV $^{-1}$) | Test Statistic (TS) value |
|-----------------------------|--|---------------------------|
| 1 | $(2.457 \pm 11.17) \times 10^{-10}$ | 0.056 |
| 1.8 | $(1.173 \pm 1.126) \times 10^{-7}$ | 1.215 |
| 2 | $(3.146 \pm 2.565) \times 10^{-7}$ | 2.077 |
| 2.2 | $(7.458 \pm 4.923) \times 10^{-7}$ | 2.973 |
| 2.4 | $(1.433 \pm 0.839) \times 10^{-6}$ | 3.592 |

TABLE 4: 95% C.L. γ -ray flux upper limit obtained from the power-law spectral modelings of Tuc-II with five different spectral indices (Γ).

| Spectral Index (Γ) | Flux upper limits in 95% C.L. (cm $^{-2}$ s $^{-1}$) |
|-----------------------------|---|
| 1 | 3.248×10^{-11} |
| 1.8 | 4.484×10^{-10} |
| 2 | 8.362×10^{-10} |
| 2.2 | 1.401×10^{-9} |
| 2.4 | 2.113×10^{-9} |

and is already implemented in the `pyLikelihood` module of `ScienceTools` as function `bayesianUL()` of python code ‘`UpperLimits.py`’. With this method, the flux upper limits in 95% C.L. is being estimated by integrating the whole likelihood profile, in which the integration was started from the lower bound of normalization parameter i.e. from $N_0 = 0$ without considering any specific distribution.

The 95% flux upper limits estimated from the semi-Bayesian method are displayed in TABLE 4 for each of the spectrum indices (Γ) considered above. In TABLE 4, we note that, the 95% C.L. γ -flux upper limit for $\Gamma = 1$ is almost 2 orders of magnitude lower than the one corresponding to $\Gamma = 2.4$. This result is consistent with our previous work for Triangulum-II (Tri-II) [66], in which we have also found that the flux upper limit in 95 % *C.L.* is increased by increasing the spectral indices.

In section 3.2, we attempted to examine the dark matter signature, hence we have modeled Tuc-II with the γ -ray spectrum from DM annihilation (DMFit function) implemented in *Fermi ScienceTools*. In that section, along with Tuc-II, we have introduced two other dwarf galaxies, namely, Ret-II and UMi and we have also followed the same analysis procedure for them that we have performed for Tuc-II (mentioned in TABLE 2).

3. THE γ -RAY SIGNATURE OF THE WIMP-ANNIHILATIONS IN TUC-II AND THE CONSTRAINTS ON THE DM MODELS

3.1. Estimation of the flux of γ -rays from Tuc-II

The expression for the differential photon flux, arising from WIMP pair-annihilations, in a DM source subtending a solid angle $\Delta\Omega$ at the observer’s location is known (e.g. [5, 67]) to be

$$\phi_{\text{WIMP}}(E, \Delta\Omega) = \Phi^{pp}(E) \times J(\Delta\Omega), \quad (2)$$

in which, $\Phi^{pp}(E)$, with the photon energy E , is the *Particle physics factor*; whereas, $J(\Delta\Omega)$ in Eq. (2) is the *Astrophysical factor* or the J-factor. For estimating the γ -ray flux from Tuc-II, we have used the same approach as we used in our previous paper [66] but in the following sections, we reproduce brief descriptions of these factors for the sake of completeness.

3.1.1. Particle physics factor

The expression for the particle physics factor that provides information regarding the properties of the initial and the final state particles in various possible WIMP pair-annihilation channels is given by [5]

$$\Phi^{pp}(E) = \frac{<\sigma v>}{8\pi m_{\text{WIMP}}^2} \sum_f \frac{dN_f}{dE} B_f. \quad (3)$$

In Eq. (3), $<\sigma v>$ denotes the thermally averaged product of the relative velocity between the WIMPs and their pair-annihilation cross-section [5]; whereas, $\frac{dN_f}{dE}$ and B_f denotes the differential photon spectrum per DM annihilation and the branching ratio of a particular WIMP pair annihilation final state ‘ f ’, respectively.

3.1.2. Astrophysical factor (J-factor)

The expression for the J-factor in Eq. (2) that contains the information regarding the astrophysical properties of the potential DM source (i.e., Tuc-II in the context of this paper), takes the form [5]:

$$J(\Delta\Omega) = J(\lambda, \theta) = 2\pi \int_0^{\theta_{\max}} \sin \theta \int_{\lambda_{\min}}^{\lambda_{\max}} \rho^2(\sqrt{\lambda^2 + d^2 - 2\lambda d \cos \theta}) d\lambda d\theta, \quad (4)$$

Where, $\rho(r)$ is the radial distribution of the DM mass-density in UFDs. In Eq. (4), λ is the line-of-sight (l.o.s) distance, d is the heliocentric distance and θ is the angle between the l.o.s and the center of UFDs, respectively.

Like in our previous paper [66], we use a simple analytical formula for the evaluation of the J-factor in this paper also. This approximate formula was originally provided in Ref. [56] from the solutions of the spherical Jeans’ equation in the particular cases of the spherical or the nearly spherical dwarf satellites at sufficiently large distances from the Sun. In our analysis, we have considered the Navarro-Frenk-White (NFW) density profile [68] for modeling the DM distribution in UFDs. This formula is given as

$$J \approx \frac{25}{8G^2} \frac{\sigma_v^4 \theta_{\max}}{dR_h^2}. \quad (5)$$

In Eq. (5), $\theta_{\max} = \arcsin(r_{\max}/d)$; r_{\max} is an estimation of the maximum galactocentric distance in the sample of the observed member stars [56] in UFDs.

The choice of θ_{\max} can restrict us to more conservative estimation of the J-factor. By considering the θ_{\max} for J-factor estimation, we assume that DM halos don’t expand beyond the r_{\max} but in reality DM halos can expand beyond it. Furthermore, The estimation of θ_{\max} depends solely on the specific observational strategies and hence it can create a bias to the dSphs.

One of the goals of this paper is to compare Tuc-II with Ret-II and UMi and for such purpose, we need to consider a uniform θ_{\max} for all the dSphs to estimate the J-factor. For our case, we have taken $\theta_{\max} = 0.5^\circ$ as a uniform angle and the choice is motivated by the point spread function (PSF) of *Fermi*-LAT. In TABLE 5, we have mentioned all the parameter values required for a numerical estimation of J-factor and its uncertainties for UFDs from Eq. (5).

TABLE 5: Different parameters to calculate the astrophysical factor (J-factor)

| Name | d (kpc) | σ_v (km sec $^{-1}$) | R_h (pc) | θ_{\max} (deg) | $\log_{10} J(\theta_{\max})$ from Eq. 5 (GeV 2 cm $^{-5}$) | $\log_{10} J(\theta = 0.5^\circ)$ from Eq. 5 (GeV 2 cm $^{-5}$) |
|--------|---------------------|------------------------------|----------------------------|-----------------------|--|---|
| Tuc-II | 57 ± 5 [39, 56] | $8.6^{+4.4}_{-2.7}$ [39] | $165^{+27.8}_{-18.5}$ [20] | 0.30° [55] | $19.14^{+0.79}_{-0.68}$ | $19.36^{+0.79}_{-0.68}$ |
| Ret-II | 30 ± 3 [56] | $3.6^{+1.0}_{-0.7}$ [49] | $32^{+1.9}_{-1.1}$ [20] | 0.20° [48] | $19.15^{+0.45}_{-0.40}$ | $19.55^{+0.45}_{-0.40}$ |
| UMi | 76 ± 3 [69, 70] | 11.61 ± 0.63 [69] | 181 ± 27 [70] | 1.37° [70] | $20.11^{+0.20}_{-0.18}$ | $19.67^{+0.20}_{-0.18}$ |

The uncertainties in $\log_{10} J$ are calculated from Eq. (5) by using the distribution of σ_v , R_h and d . For estimating the uncertainties, we have developed a code which is intended to find limiting values of the J-factor by a Montecarlo algorithm, with the input being the values of the variable σ_v , R_h and d , along with their respective limits. In that code, firstly we have generated random numbers with a user-defined distribution. For our purpose, we have taken asymmetric normal distribution about the mean with two different values of the standard deviation on each side of the mean, because many of the given parameters lie in an asymmetrical limit. The program generates the distribution by the use of Smirnov Transform on a set of uniformly distributed random numbers. Next, we have used the Montecarlo algorithm to generate the values of the variables σ_v , R_h and d within the tolerance limits (95% C.L. for our case) of limiting values.

TABLE 6: Comparison of $\log_{10} J$ ($\theta = 0.5^\circ$) between our calculation and Pace *et al.*, 2018[71] and Evan *et al.*, 2016[56] result

| Name | Our calculation | Pace <i>et al.</i> , 2018[71] | Evan <i>et al.</i> , 2016[56] |
|--------|--|--|--|
| Tuc-II | $19.36^{+0.79}_{-0.68}$ ($\text{GeV}^2 \text{ cm}^{-5}$) | $18.84^{+0.55}_{-0.49}$ ($\text{GeV}^2 \text{ cm}^{-5}$) | $19.05^{+0.87}_{-0.58}$ ($\text{GeV}^2 \text{ cm}^{-5}$) |
| Ret-II | $19.55^{+0.45}_{-0.40}$ ($\text{GeV}^2 \text{ cm}^{-5}$) | $18.95^{+0.38}_{-0.36}$ ($\text{GeV}^2 \text{ cm}^{-5}$) | $18.71^{+0.84}_{-0.32}$ ($\text{GeV}^2 \text{ cm}^{-5}$) |
| UMi | $19.67^{+0.20}_{-0.18}$ ($\text{GeV}^2 \text{ cm}^{-5}$) | $18.89^{+0.16}_{-0.20}$ ($\text{GeV}^2 \text{ cm}^{-5}$) | $19.15^{+0.25}_{-0.24}$ ($\text{GeV}^2 \text{ cm}^{-5}$) |

Previously, several pieces of literature have ([39, 47, 56, 71]) also estimated the J-factor value of Tuc-II and our estimated J-factor is slightly higher compared to those studies, but all of these studies have pointed out the large uncertainty in J-factor of Tuc-II. In TABLE 6, we have compared our estimated J factor with that of Pace *et al.*, 2018 ([71]) and Evan *et al.*, 2016 ([56]), respectively.

For Tuc-II and Ret-II, both our work and Evan *et al.*, 2016 ([56]) have used the identical kinematics data but the differences in result mainly arise from the choice of halo profile of DM distribution. Evan *et al.*, 2016 ([56]) preferred the $r_s = 5R_h$ assumption of halo profile to calculate the J-factor value and their values are mentioned in TABLE I of their paper. However, in case of UFDs, very few numbers of stars have been detected and that insufficient kinematics data lead to difficulties in understanding the DM distribution in UFDs. So, instead of $r_s = 5R_h$ assumption, we have adopted the infinite halo profile from Evan *et al.*, 2016 ([56]), where DM density (ρ) is $\propto r^{-1}$. Moreover, our error estimation is possibly different from the error obtained by Evan *et al.*, 2016 ([56]). From TABLE 6, it is then evident that the estimation of J-factor is directly dependent on the assumption of DM halo profile and also on the method of error estimation.

It is also important to note that our estimated J-factor for Ret-II differs by almost an order of magnitude than Evan *et al.*, 2016 ([56]) and it also changes the ranking of dSphs with respect to that obtained by Evan *et al.*, 2016 ([56]). Differences in the DM profiles are responsible for such discrepancies. One of the assumptions of our used analytical formula is that all dSphs lie at sufficiently large distances. But, Ret-II is one of the nearest dSphs to us (≈ 30 Kpc [56]) and it leads to a large difference between our obtained result and Evan *et al.*, 2016 ([56]), whereas Tuc-II lies at a sufficiently large distance and that reduces the difference between these two results.

In the following sections, we have used the J-factor at $\theta_{max} = 0.5^\circ$ for dSphs.

3.2. DM annihilation Constraints from Tuc-II

3.2.1. Searching for γ – ray emission due to DM Annihilation from Tuc-II

In this subsection, we have fitted the possible γ -ray flux from Tuc-II in terms of the flux arising out of the pair-annihilation of the WIMPs by employing a full-scale MC simulation package DMFit [54, 72], as implemented in the **ScienceTools**. The DMFit package is based on the particular set of MC simulations of hadronization and/or decay of the annihilation products as used by the DarkSUSY team [54, 72] by means of the Pythia 6.154 [73] event generator. With this γ -ray spectrum from DM annihilation, we defined Tuc-II as a point source and the significance of the Tuc-II is estimated by the ΔTS method as we already mentioned in section 2.3.

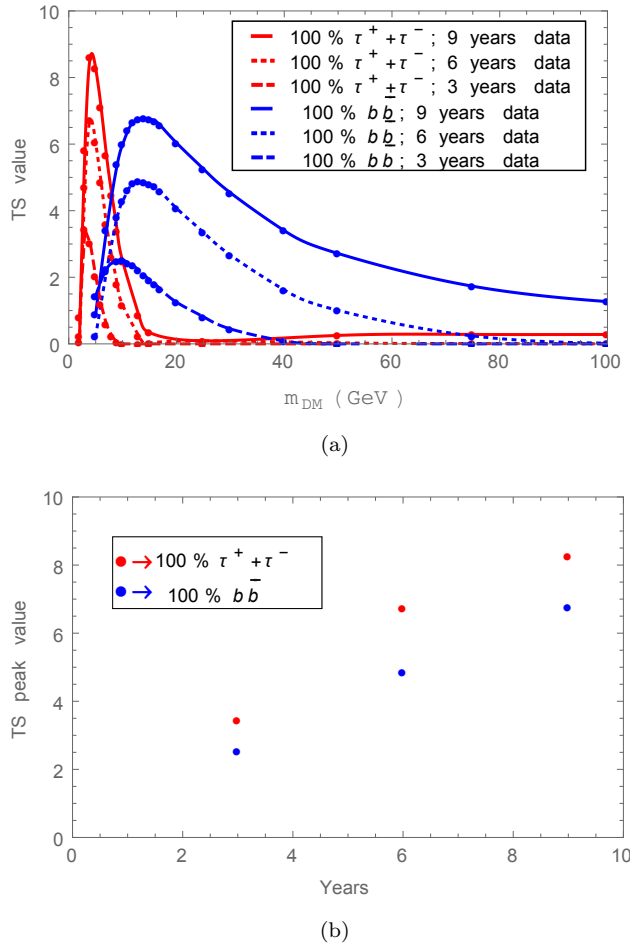


FIG. 2: (a) Variation of observed TS values of Tuc-II as a function of DM mass (m_{DM}) results from two WIMP pair annihilation channels; 100% $b\bar{b}$ (blue) and 100% $\tau^+ + \tau^-$ (red) with three different time periods of *Fermi*-LAT data. (b) The observed TS peak of the excess γ -ray emission from the direction of Tuc-II for three different time intervals of *Fermi*-LAT data, whereas, the red and blue markers denote the TS peak for 100% $b\bar{b}$ and 100% $\tau^+ + \tau^-$ annihilation channels, respectively. The colors and the line-styles of different curves are indicated in the diagram.

In Fig. 2(a), we have shown the detection significance of γ -ray emission, i.e the TS values from the direction of Tuc-II as a function of DM mass (m_{DM}) for two pair annihilation channels, 100% $b\bar{b}$ and 100% $\tau^+ + \tau^-$. In that same figure, we have also compared the detected TS values from Tuc-II for three, six and nine years of *Fermi*-LAT data and for such purpose we have applied the same analysis method on these three dataset. In Fig. 2(b), we have shown that the TS peak of Tuc-II is increased with the larger dataset and the same nature is followed by both annihilation channels. Even though the observed significance is faint (i.e. less than TS=25) to claim anything strongly, the most encouraging part of this result is that TS peak of Tuc-II is continuously increasing with time and in future this could possibly lead us to a detection of a real signal either from any astrophysical source or from DM annihilation. From Fig. 2(a), we can observe that with nine years of *Fermi*-LAT data, the TS value peaks at $m_{DM} = 14$ GeV for 100% $b\bar{b}$ annihilation channel, whereas for 100% $\tau^+ + \tau^-$ it peaks at $m_{DM} = 4$ GeV.

There are some studies which have previously analyzed Tuc-II with 6 or 7 years of *Fermi*-LAT data[33, 45–47]. In our analysis we have studied it with nine years of *Fermi*-LAT data. The increase in TS values of Tuc-II with 9 years of *Fermi*-LAT data can possibly come from a larger dataset. Thus, this increase in the γ -ray emission with the largest possible available dataset seems encouraging in indirect detection of DM signal.

For both the power-law and the DM annihilation spectra, the best-fitted spectra have been obtained from likelihood ratio test (i.e. $TS = -2 \ln (L_{(\max,0)} / L_{(\max,1)})$). We have found that the best-fitted TS value is significantly improved with dark matter annihilation hypothesis. Moreover, the p-value (p-value is the probability of getting

TABLE 7: Summary of test statistics (TS) and Δ TS for the two source models considered in this paper: power law (PL) for $\Gamma = 2.4$ and the best-fitted dark matter spectrum (DM) corresponds to its highest TS value (in our case 100% $\tau^+\tau^-$ channel at DM mass= 4 GeV)

| Our source | TS for PL | σ ($\approx \sqrt{TS}$) for PL | p-value for PL | TS for DM | σ ($\approx \sqrt{TS}$) for DM | p-value for DM | Δ TS (DM-PL) |
|------------|-----------|---|----------------|-----------|---|----------------|---------------------|
| Tucana-II | 3.592 | 1.895 | 0.05 | 8.60998 | 2.934 | 0.003 | 5.01798 |

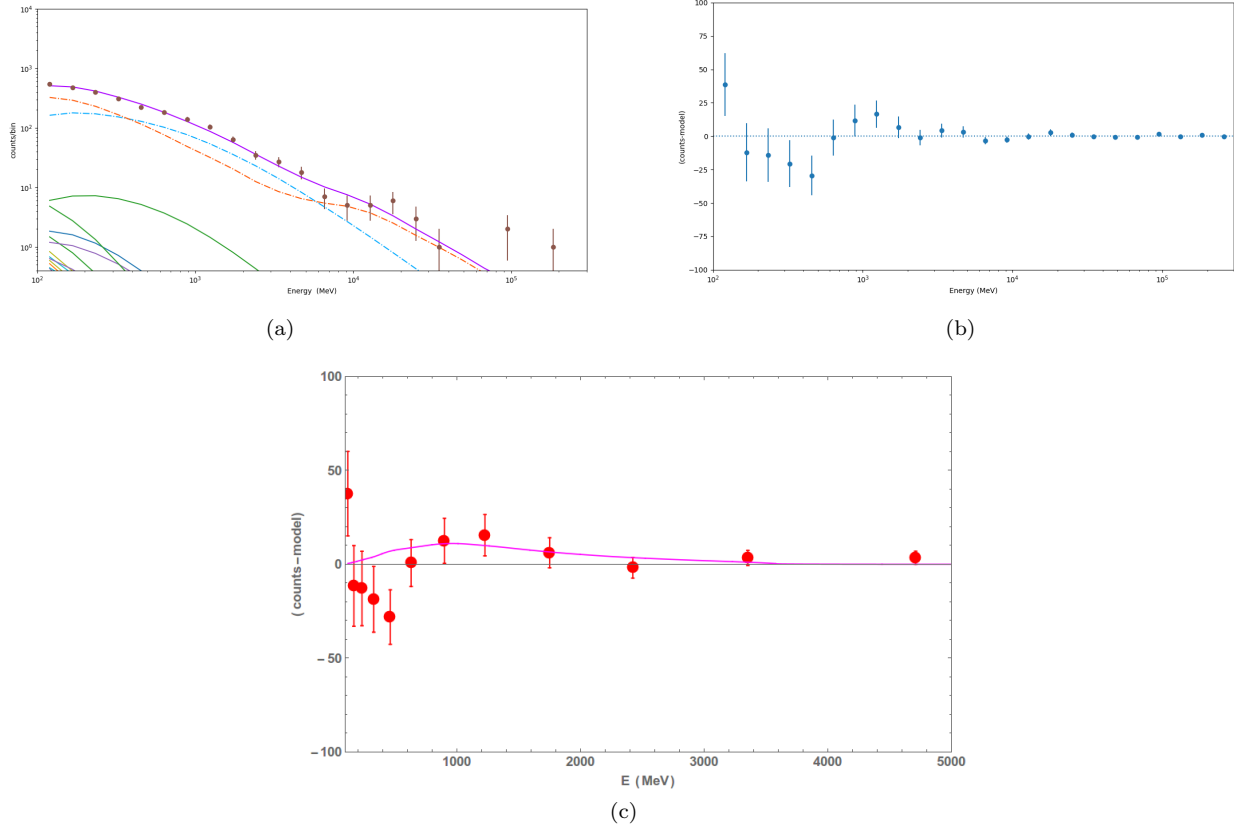


FIG. 3: Spectral fit to the counts (Fig. 3(a)) and the corresponding residual plot (Fig. 3(b)) for a $1^\circ \times 1^\circ$ ROI centred on Tuc-II. In Fig. 3(a), the solid purple curve displays the best-fit total spectrum, along with the corresponding LAT-observed data points (in brown); the dot-dashed sky blue and orange curves display the galactic diffuse background and the isotropic background component, respectively. In Fig. 3(c), we show the best-fitted dark matter spectra for 100% $\tau^+\tau^-$ annihilation channel at $m_{DM} = 4$ GeV with a magenta solid line and the residual plot from Fig. 3(b) between 100 MeV to 5 GeV energy range is overplotted here as the red points with errorbars.

“signal-like” data obtained from the background excess) of local significance is also reduced with DM annihilation spectrum. These details are mentioned in TABLE 7. This table shows that our results may favor the dark matter annihilation hypothesis over its astrophysical connection with the excess obtained from the location of Tuc-II. But it is also important to note that for both power-law ($-\log(\text{Likelihood}) = 11460$) and DM annihilation hypothesis ($-\log(\text{Likelihood}) = 11562$), we have obtained a comparable $-\log(\text{Likelihood})$ value. Therefore, we are not in a position to firmly rule out the astrophysical connection over the DM annihilation hypothesis. Hence we can conclude that our results, at best, show a hint of a DM signal from Tuc-II.

In section 2.3, we have performed the Fermi-LAT analysis on $10^\circ \times 10^\circ$ ROI around Tuc-II but with such large region of the sky, it is quite impossible to identify any interesting features at the location of Tuc-II. So, in this section to study the gamma-ray excess possibly generated from Tuc-II, we have repeated the binned likelihood analysis for much smaller ROI i.e. for $1^\circ \times 1^\circ$ ROI centered on Tuc-II. Here we have not included Tuc-II in our source model and

for other sources the best-fitted model parameters from $10^\circ \times 10^\circ$ ROI fitting have been used for the likelihood analysis.

Fig. 3(a) shows the spectral fit per energy bin of all the sources within the aforementioned ROI except for Tuc-II, along with the isotropic and the galactic diffuse background components. The corresponding residual plot in the given ROI is shown in Fig. 3(b). In Fig. 3(b), the contribution from the Tuc-II has not been taken into account and \sim above 500 MeV we could observe an excess from the residual plot.

In Fig. 3(c), we have shown the best-fitted DM spectrum of Tuc-II with magenta solid line and the points from residual plot (Fig. 3(b)) between 100 MeV to 5 GeV are overplotted with red points. Here, we have chosen the best-fitted DM spectrum for 100% $\tau^+\tau^-$ annihilation channel at DM mass= 4 GeV, as it produces the highest TS value of Tuc-II (see Fig. 2(a,b)). From Fig. 3(c), we can observe that in between 500 MeV to 5 GeV energy range, the best-fitted DM annihilation spectra produces a good fit to the bump of residual excess with a p-value of 0.0086 (Here p-value is associated with the *chi-square goodness of fit*). This fitting hints that the bump in the residual plot (Fig. 3(b)) could be due to the DM annihilation in Tuc-II. However, our obtained TS values are lower compared to the *Fermi*-LAT threshold detection limit, so we are not in a position to completely eliminate the possible contribution from any statistical fluctuation or its connection with nearby unmodeled astrophysical sources. In subsection 3.2.2, we discuss this aspect in detail. But our study hints that with more detailed analysis and with larger periods of data, Tuc-II could possibly lead us to a new detection in DM signal from dSphs.

3.2.2. Distribution of the Excess obtained from γ -ray spectra of DM annihilation

TABLE 8: A list of BZCAT and CRATES sources that lie within 1° of Tuc-II. J225455-592606 is detected in both catalogs, so we listed it with the CRATES coordinates.

| Our source | Nearby sources from BZCAT and CRATES catalog | Distance to the Tuc-II ($^\circ$) |
|------------|--|-------------------------------------|
| Tucana-II | J 225134-580103 | 0.55 |
| | J 225008-591029 | 0.66 |
| | J 225455-592606 | 0.95 |

TABLE 9: The summary test statistics (TS) values of Tuc-II and other three nearby sources from CRATES and BZCAT catalog are listed here. For Tuc-II we have chosen the TS peak values for 100% $\tau^+\tau^-$ annihilation channel with DM mass=4 GeV and the other three nearby sources (within 1° for Tuc-II) are modeled with power-law spectra of $\Gamma = 2.2$ [74].

| Year | Tuc-II | J 225134-580103 | J 225008-591029 | J 225455-592606 |
|------|--------|-----------------|-----------------|-----------------|
| 9 | 7.597 | 3.043 | 3.863 | 1.391 |
| 6 | 5.600 | 1.04 | 1.40 | 0.0799 |
| 3 | 3.043 | 0.066 | 0.0377 | 0.031 |

In subsection 2.3 and 3.2.1, we have estimated the TS value by Δ TS method but have not checked any nearby background fluctuation which can also be responsible for the significance obtained from the location of Tuc-II. More importantly, from our analysis, we have obtained a very faint hint of excess from Tuc-II, so to claim its connection with DM annihilation, we need to carefully quantify the cause of this excess.

There is a possibility that the excess obtained from Tuc-II could come either from the nearby unresolved sources or from the deficiency of background models. However, from Fig. 1(a) it is evident that two diffuse background models show a good-fitting to $10^\circ \times 10^\circ$ ROI around the centered position of Tuc-II, so it is unlikely that the γ -ray excess from Tuc-II could originate from the deficiency of background models.

The γ -ray excess from Tuc-II can also plausibly arise from a number of nearby faint γ -ray sources including star-forming galaxies [75, 76], radio galaxies [77], blazars [78] and millisecond pulsars [79]. Among all types of different background sources, blazars are the most promising candidates to explain the background fluctuations [74]. Star-forming and radio galaxies can also provide a non-negligible contribution in γ -ray sky. But at the high-latitude gamma-ray sky, blazars are the most numerous point sources and they are thought to be the main source of anisotropy

in the extragalactic gamma-ray background [80–85].

The Fermi-LAT collaboration has also studied a large portion of the blank sky and has pointed out that most of the region showed an excess of $TS > 8.7$ with respect to the predicted diffuse background model [35]. Carlson *et al.*, 2015 [74] have also argued that unresolved blazars, radio galaxies, star-forming galaxies are mostly responsible for such excess and a proper multiwavelength study can reduce contamination from these sources. They have also concluded that a major portion of the excess is likely to be responsible for most of the observed deviations from Fermi’s diffuse background model.

In this subsection, we have tried to perform a more detailed study to investigate the possible reason for obtaining a TS value of ~ 8.6 from the location of Tuc-II. We have chosen two multiwavelength blazar catalogs i.e. BZCAT [86] and CRATES [87]. BZCAT contains nearly 3149 known blazars and 2274 of which are located at high galactic latitude (i.e. $|b| > 30^\circ$) and CRATES detected more than 11,000 bright flat-spectrum radio sources. Within 1° of Tuc-II, we have found three radio sources from the CRATES catalog and one blazar from the BZCAT catalog. The source from BZCAT catalog has also been detected by CRATES. For our investigation, we have only considered CRATES sources (J225134-580103, J225008-591029 and J225455-592606), which are located within a 1° from Tuc-II because any blazars, radio or star-forming region beyond 1° possibly would not produce any effective changes to local significance of dSphs [74]. The list of CRATES sources within 1° of Tuc-II is mentioned in TABLE 8.

We have modeled these three sources with the power-law spectrum of $\Gamma=2.2$ [74] and have determined the TS values of these sources for three different time periods of Fermi-LAT data. All the results are shown in TABLES 9. The result of this analysis is that by including these three sources, the significance of Tuc-II is only decreased by $\sim 10\%$.

In order to check the distribution of excess obtained from Tuc-II, we have created the $5^\circ \times 5^\circ$ the residual TS map (100 MeV - 300 GeV) around Tuc-II with ‘*gttsmap*’. In this process, the model parameters of all the sources within ROI of $10^\circ \times 10^\circ$ were kept fixed to their best-fitted values obtained from the binned likelihood analysis on 9 years of Fermi-LAT data and the normalization parameters of both the galactic and isotropic components were left free. We have run the same process for three cases: First (Fig. 4(Left)); we have not included Tuc-II and three nearby BZCAT and CRATES sources, that lie within a 1° of Tuc-II, to the source model. Second (Fig. 4(Middle)); we have included the Tuc-II to source model but not the other three nearby radio BZCAT and CRATES sources. Third (Fig. 4(Right)); we have included the Tuc-II and also three BZCAT and CRATES sources to the source model. Here, for Tuc-II the best fitted parameters obtained from dark matter annihilation spectra (i.e. 100% $\tau^+\tau^-$ channel at DM mass=4 GeV) has been used to generate the second and third residual TS map.

From Fig. 4(Left), it is directly evident that there is a hint of excess from the location of Tuc-II. It is also important to note that whenever we have included Tuc-II to our source model, the localized excess around the position of Tuc-II is significantly reduced (Fig. 4(Middle)). We have roughly denoted the region of excess localized at around Tuc-II with a green box and the name of all sources within a 1° from Tuc-II are mentioned with a white cross. In Fig. 4(Right), after including Tuc-II as well as three CRATES sources to the source models, we have not found any delocalized excess within 1° from Tuc-II. It points out that breakdown of diffuse background is possibly not responsible for such excess, otherwise, we should observe a spatially-correlated excess around Tuc-II in residual TS map. Our performed test indicates that neither the nearby CRATES and BZCAT sources nor the diffuse backgrounds are solely responsible for the faint excess from the location of Tuc-II. All of these tests just strengthen the connection of the emission from Tuc-II with the dark matter annihilation signal.

Amongst newly discovered UFDs, Ret-II is one of the most promising sources of indirect DM detection because several literature have already pointed out the dark matter annihilation connection with a faint emission obtained from the location of Ret-II ([33, 45, 47, 51–53]). But recently Geringer-Sameth *et al.*, 2018 [88] has argued whether there is any astrophysical connection with the signal obtained from Ret-II. They find that it is very likely for Ret-II to host a gamma-ray source. Like Ret-II, we have only observed a very faint emission from the Tuc-II and for such low excess emission, may be a more detailed analysis need to be performed to firmly conclude its connection with dark matter annihilation signal.

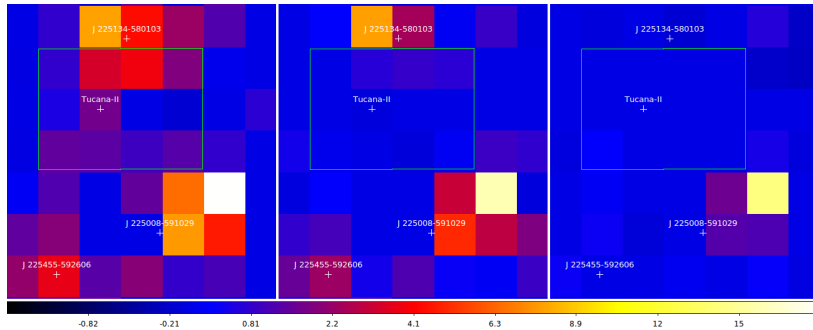


FIG. 4: Residual TS maps (100 MeV - 300 GeV) of $5^\circ \times 5^\circ$ regions centered at Tuc-II extracted from the $10^\circ \times 10^\circ$ ROI data around Tuc-II. The image scale of TS map is 0.25 pixel^{-1} . In left Fig., Tuc-II and the three CRATES sources are not included in the source model; in middle Fig., Tuc-II is included in the source model but not the other three CRATES sources; in right Fig., Tuc-II and the three CRATES sources have been included in the source model.

3.2.3. Possible DM annihilation Constraint on theoretical DM Models with 9 years of Tuc-II Fermi-LAT data

Since with dark matter annihilation spectra, our obtained TS peak value for $\tau^+\tau^-$ annihilation channel is weaker than Fermi-LAT' threshold detection limit (i.e. $\text{TS} < 25$), in this section we estimated γ -ray flux upper limit in 95 % C.L. from Tuc-II by semi-Bayesian method [65], as described in subsection 2.3 of this paper. By employing the γ -ray spectrum from DM annihilation, we could also calculate the upper limits to the thermally averaged pair-annihilation $\langle \sigma v \rangle$ of the WIMPs with the variation of the plausible WIMP masses (m_{DM}), for various important pair-annihilation final states (f), i.e. for each of the possible important channels in which WIMP annihilations might take place to produce γ -rays [7]. We have considered five supersymmetry-motivated pair annihilation final states [7], namely 100% $b\bar{b}$, 80% $b\bar{b} + 20\% \tau^+\tau^-$, the 100% $\tau^+\tau^-$, 100% $\mu^+\mu^-$ and 100% W^+W^- , respectively. The variation of such 95 % γ -ray flux upper limits of Tuc-II obtained from semi-Bayesian method and the relative upper limits to their annihilation $\langle \sigma v \rangle$ with increasing WIMP masses are displayed in Fig. 5(a,b), separately for each of the annihilation channels mentioned above.

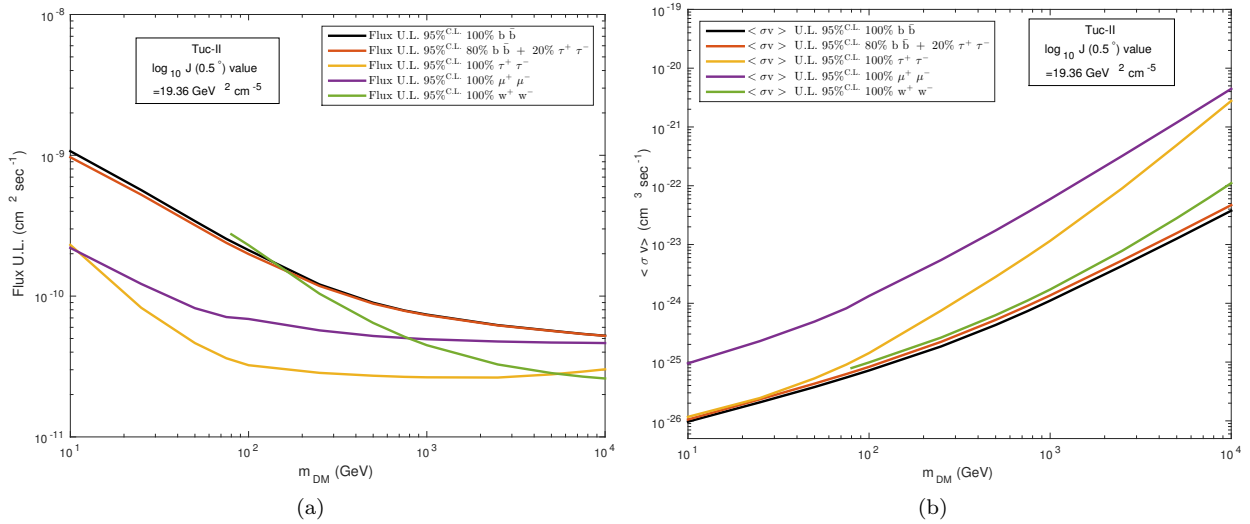


FIG. 5: Variations of (a) the 95% C.L. γ -ray (integral) flux upper limits of Tuc-II and (b) the corresponding pair-annihilation $\langle \sigma v \rangle$ of the WIMPs with their increasing masses (m_{DM}), as estimated for various annihilation final states “f” (indicated in the diagram) by using the DM annihilation function with semi-Bayesian likelihood method. Each of these results is estimated for the median $J(0.5^\circ)$ -factor value of Tuc-II (mentioned in TABLE 5.).

In Figs.6 (a,b) and 7, we have displayed the DM annihilation function-determined 95% C.L. upper limit of the thermally averaged WIMP pair-annihilation $\langle \sigma v \rangle$, as a function of the WIMP mass (m_{DM}) for its median J -factor

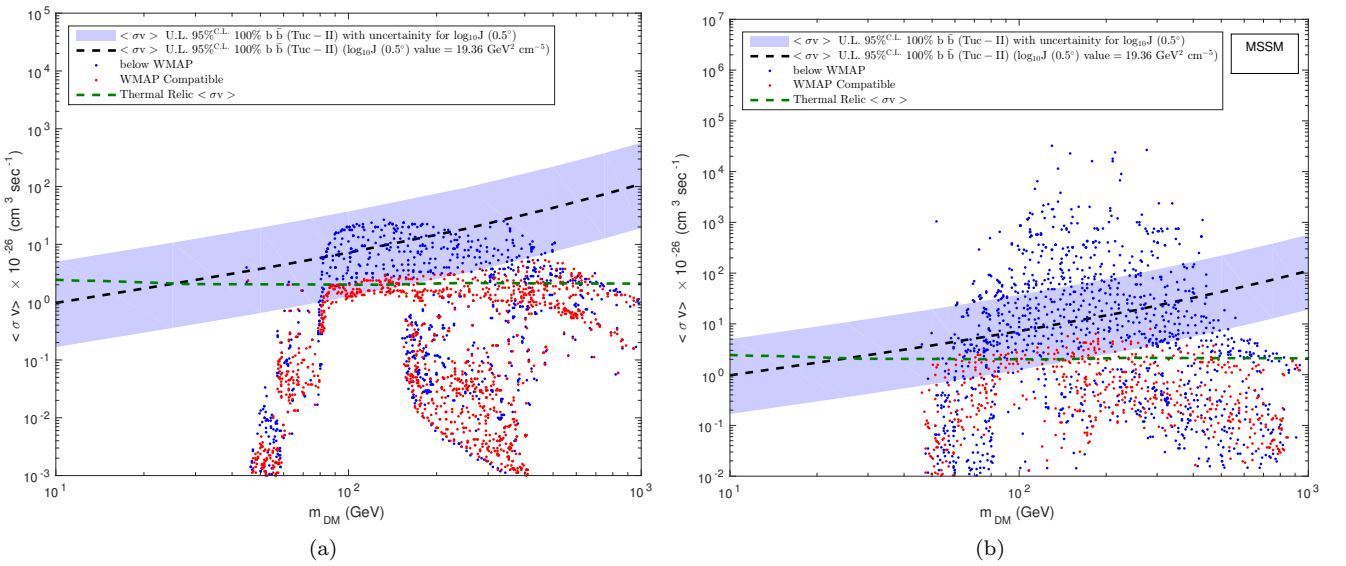


FIG. 6: Variation of 95% C.L. upper limit of the WIMP pair-annihilation $\langle \sigma v \rangle$ with increasing m_{DM} for $b\bar{b}$ annihilation final states of Tuc-II displayed in $(m_{DM}, \langle \sigma v \rangle)$ plane for J-factor with its uncertainties. The shaded band represents the uncertainty in the DM density profiles in the Tuc-II. In the figures, the $\langle \sigma v \rangle$ are compared with points derived from (a) the mSUGRA and of (b) the MSSM models [5]. In those later models, the red points correspond to thermal relic density compatible with the WIMP data. The blue points represent higher $\langle \sigma v \rangle$, and correspondingly lower thermal relic densities, obtained by assuming certain additional nonthermal production mechanisms to contribute to WIMP production, while the WIMPs still comprise all of the DM. In both the figures, we have also overplotted the relic abundance (or thermal) cross section ($2.2 \times 10^{-26} \text{ cm}^3 \text{ s}^{-1}$) estimated by Steigman *et al.*, 2012 [89] and it is displayed as green dashed line.

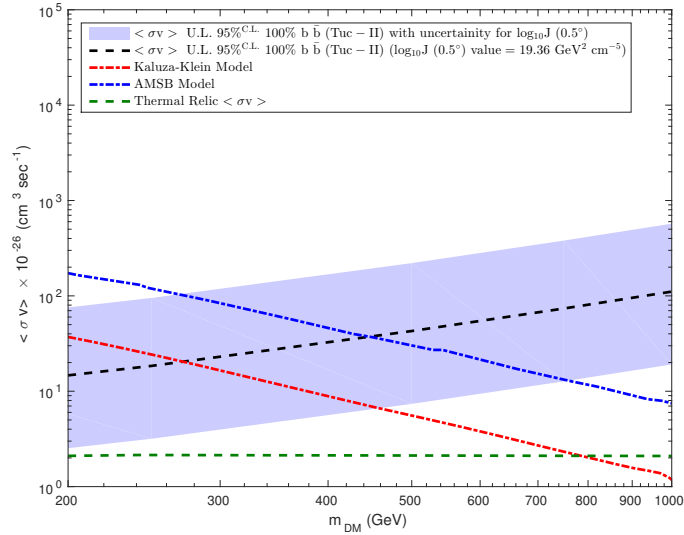


FIG. 7: A comparison between the γ -ray spectrum from DM annihilation for 95% C.L. upper limit of $\langle \sigma v \rangle$ vs. m_{DM} curve from Tuc-II and the theoretical $\langle \sigma v \rangle$ vs. m_{DM} curves obtained from the AMSB and the Kaluza-Klein UED models. The shaded band represents the uncertainty in the DM density profiles in the Tuc-II for $b\bar{b}$ annihilation final states. We have also overplotted the relic abundance (or thermal) cross section ($2.2 \times 10^{-26} \text{ cm}^3 \text{ s}^{-1}$) estimated by Steigman *et al.*, 2012 [89] and it is displayed as green dashed line.

and J-factor uncertainties. Only the $\langle \sigma v \rangle$ upper limit in 100% $b\bar{b}$ annihilation channel has been considered in these figures as they are found to put the most stringent limits on the parameter space of the models. In Figs. 6(a,b) and 7, the horizontal dashed green line denotes to the relic abundance (or thermal) cross section estimated by Steigman *et. al.* [89]. These results are then compared with the $\langle \sigma v \rangle$ values obtained for various WIMP masses (m_{DM}) from four theoretical DM models, namely the minimal Supergravity (mSUGRA; in Fig. 6(a)) [90] model, the

Minimal Supersymmetric Standard Model (MSSM; in Fig. 6(b)) [91] model, the Anomaly Mediated Supersymmetry Breaking model (AMSB) [92] (in Fig. 7) model and the lightest Kaluza-Klein particle of Universal Extra Dimensions (UED) model [93–95] (in Fig. 7), respectively.

In mSUGRA model, the supersymmetry breaking parameters are defined at the order of grand unification scale $\sim 2 \times 10^{16}$ GeV i.e. at high energy scale, whereas, for MSSM model, the supersymmetry breaking parameters are defined at the low energy scale i.e. at electropotential scale. For AMSB model, the supersymmetry breaking parameters are considered to produce winos; these winos or wino-like neutralino basically are the supersymmetric fermionic partner of the gauge bosons from Standard Model. At about 2 TeV wino mass, their thermal relic density matches with the universal DM density, on the other hand, several non-thermal DM production mechanisms can explain the winos with comparatively less massive DM particles [5]. In Kaluza-Klein model, its first order excitation term of U(1) hypercharge gauge boson is connected to the DM candidate and at about 700 GeV DM mass, this model can define the thermal relic abundance from their DM density. In Figs. 6(a,b) the blue points in both of the models represent the low thermal relic density with additional nonthermal production mechanisms for the WIMPs to describe the universal matter density, on the other hand, the red points are consistent with the cosmological thermal relic density [5].

From the Figs. 6 (a,b) and 7, it is immediately evident that lowest limit of the shaded band of Tuc-II would impose a very strong constraint on the parameter spaces of the popular theoretical WIMP models. In Figs. 6(a,b), it is interesting to note that, for the median $J(0.5^\circ)$ -factor of Tuc-II (i.e. for $\log_{10} J(0.5^\circ) = 19.36$ GeV 2 cm $^{-5}$), the upper limits of $\langle \sigma v \rangle$ considerably constrain the blue points in both MSSM and mSUGRA model, while the J -factor uncertainty band of Tuc-II have already begun to constrain the red points in both the models. Fig. 7 shows that the upper limit of $\langle \sigma v \rangle$ from Tuc-II for the median $J(0.5^\circ)$ -factor (i.e. for $\log_{10} J(0.5^\circ) = 19.36$ GeV 2 cm $^{-5}$), as determined from Eq. (5) above disfavors the AMSB and the Kaluza-Klein UED models for masses < 500 GeV and < 300 GeV respectively.

The large uncertainties in J -factor of Tuc-II comes from its insufficient kinematics data. With more precise observation of the internal structure of Tuc-II, in future we should definitely reduce this uncertainty band to a possible single upper limit curve of $\langle \sigma v \rangle$ and that might improve the constraint limit on beyond Standard Model. This result would then possibly signify the hint of new physics in the field of indirect dark matter detection.

3.2.4. Comparison of the constraints on the DM annihilation cross section ($b\bar{b}$ channel) obtained from Tuc-II, Ret-II and UMi

In this section, we have compared the upper limit of $\langle \sigma v \rangle$ obtained from Tuc-II with two other UFDs, namely UMi and Ret-II, respectively. In Fig. 8(a) we have shown the 95% C.L. upper limit of the WIMP annihilation $\langle \sigma v \rangle$ for only $b\bar{b}$ channel obtained by the analysis of nine years of LAT-data of Tuc-II, UMi and Ret-II. For estimating the 95% C.L. $\langle \sigma v \rangle$ upper limit of these two dwarfs, we have performed the same analysis method that we have applied for Tuc-II (mentioned in TABLE 2). In Fig. 8(b), we have compared the upper limit of the $\langle \sigma v \rangle$ obtained from Tuc-II for its two J -factors, i.e. for $J(\theta_{max})$ and $J(0.5^\circ)$, respectively. From Fig. 8(b), it is also evident that $\langle \sigma v \rangle$ upper limit of Tuc-II estimated for $J(0.5^\circ)$ would produce a more stringent limit than $J(\theta_{max})$ on ($\langle \sigma v \rangle$, m_{DM}) space.

In Figs. 8(a,b) the dashed lines correspond to the median value of J -factor, while the shaded regions depict the range of uncertainty in J -factors of each of the UFDs. In the case of UFDs, very few numbers of stars have been detected so far which is the main obstacle in understanding the DM distribution in UFDs. The large uncertainty bands in Tuc-II basically represent our inadequate knowledge of its internal structure.

It may be of some interest to note that, in case of Ret-II, several recent studies have detected a slight excess in γ -emission [33, 45, 47, 51–53]. Though the significance of excess emission from Ret-II is quite lower than *Fermi*-LAT’s threshold value for detection, this excess emission is suspected to be the evidence of WIMP annihilation in Ret-II [33, 52, 53, 96].

Compare to Ret-II and UMi, Tuc-II indicates larger uncertainties in DM density profile and from Fig. 8(a), we could distinctly observe an overlapping region among the Ret-II, Tuc-II and UMi in parameter space of ($\langle \sigma v \rangle$, m_{DM}). So, in view of the indirect DM search, it is not possible to favor Tuc-II over other two dSphs but from Fig. 8(a), it is also evident that above $m_{DM} \sim 100$ GeV, Tuc-II and Ret-II show a comparable limits on ($\langle \sigma v \rangle$, m_{DM}) space for their median $J(0.5^\circ)$ values.

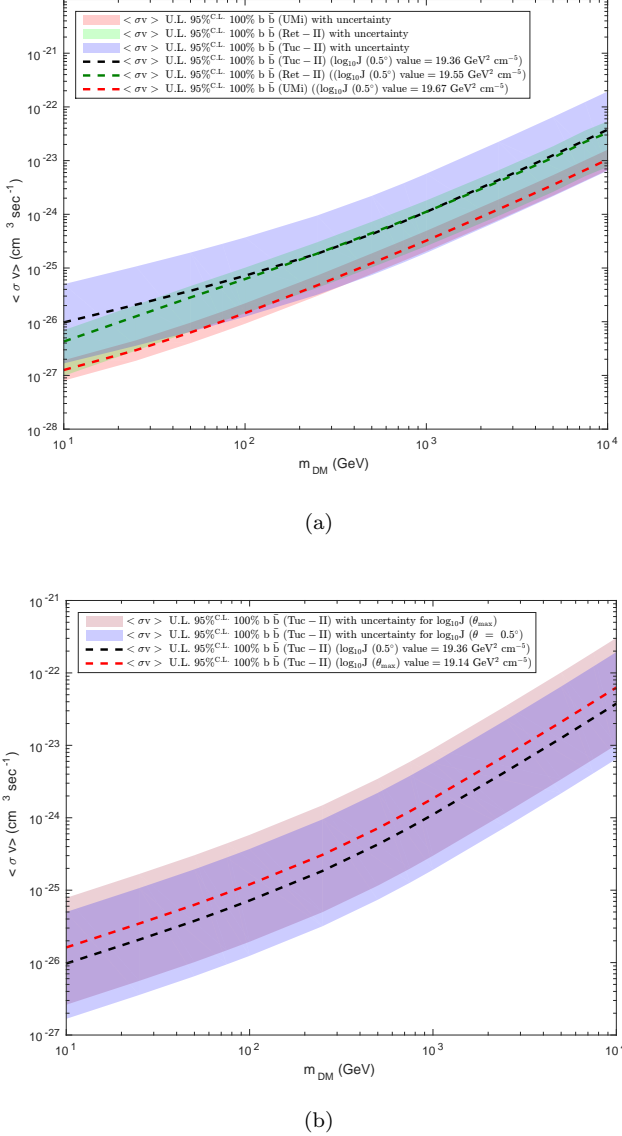


FIG. 8: Variations of (a) 95% C.L. upper limit of the WIMP pair-annihilation $\langle \sigma v \rangle$ with increasing m_{DM} for $b\bar{b}$ annihilation final states of Tuc-II, Ret-II and UMi displayed in $(m_{\text{DM}}, \langle \sigma v \rangle)$ and (b) 95% C.L. upper limit of the WIMP pair-annihilation $\langle \sigma v \rangle$ with increasing m_{DM} for $b\bar{b}$ annihilation final states of Tuc-II for two J-factors, i.e. for $J(\theta_{\text{max}})$ and $J(0.5^\circ)$, respectively. The shaded bands represent the uncertainty in the DM density profiles of UFDs and the dashed line denotes the upper limit of $\langle \sigma v \rangle$ in 95 % C.L. corresponds to median J-factor from TABLE 5. The colors and the line-styles of different curves are indicated in the diagram.

4. CONCLUSIONS AND DISCUSSION

In this paper, we have analyzed nearly nine years of *Fermi*-LAT γ -ray data from one of the recently discovered UFDs, namely Tuc-II, with the aim of detecting the signatures of self-annihilation of the WIMPs that are usually believed to be the constituent particles of DM within the UFDs/dSphs. We have found a very faint γ -ray emission from Tuc-II with both Power law and γ -ray spectrum from DM annihilation. It is interesting to note that, with γ -ray spectrum from DM annihilation, we have shown the variation of detected TS values from Tuc-II for various

DM masses and have found that with nine years of *Fermi*-LAT data TS value peaks at $m_{DM} \sim 14$ GeV for 100% $b\bar{b}$ annihilation channel, whereas for 100% $\tau^+\tau^-$ it peaks at $m_{DM} \sim 4$ GeV. In our Galactic Center, the m_{DM} between 25 GeV - 70 GeV for $b\bar{b}$ annihilation channel and m_{DM} between 8 GeV - 15 GeV for $\tau^+\tau^-$ annihilation channel play an important role to interpret the γ -ray emission resulting from WIMP annihilation [97–101]. In our analysis for Tuc-II, the TS peaks obtained for the m_{DM} for two annihilation channels are slightly lower than the DM mass range needed to explain the DM interpretation in Galactic Center.

We have also shown that this excess is increased for larger periods of data and that increase in source significance for TS peak value is roughly proportional to $\sim \sqrt{t}$ [102]; where t is the time periods of data. The most interesting part of the result is that the cumulative increase in TS peak values of Tuc-II with larger periods of data which can possibly hint at presence of any real signal either from an astrophysical source or from DM pair annihilation. In case of Ret-II, several studies [33, 45, 47, 51–53] based on *Fermi*-LAT data analysis have already observed an excess emission from the direction of Ret-II and this makes it as one of the most promising DM-rich UFDs. In indirect DM detection, the hints of increasing γ -ray excess from some particular dSphs (Tuc-II for our case) may lead us to a new direction of DM physics.

By assuming the γ -ray spectra for DM annihilation to 100% $\tau^+\tau^-$ channel, we have obtained a p-value ≈ 0.003 towards Tuc-II location and it suggests that the excess obtained from Tuc-II could come from the rare statistical fluctuation in background. More importantly, in Fig. 1(a), we have shown that the background diffuse models produced a good-fit to $10^\circ \times 10^\circ$ ROI around Tuc-II and from TS map (Fig. 4) it is also evident that the excess obtained from Tuc-II is localized. Otherwise, there would be a spatially correlated excess around Tuc-II. Apart from that, one of the most tantalizing explanations of such excess is the presence of any nearby unresolved bright sources. Among all types of unresolved background sources, blazars are assumed to be the most likely candidates to emit γ -ray emission just below the *Fermi*-LAT's threshold detection. Searching from the BZCAT and CRATES catalog, we have found that there are three radio sources within 1° of Tuc-II and amongst all the most nearby source (J225455-592606) lie at 0.55° away from Tuc-II. Thus it makes very unlikely that the excess from Tuc-II location would be highly contaminated by these sources. All of our results give a hint of a dark matter signal from Tuc-II. At present, with nine years of data, the obtained emission from Tuc-II is weaker than *Fermi*-LAT's threshold detection. But from our work, we have also found that the significance of Tuc-II is increased with increase in time periods of data. So, in future, with even more time periods of data and with better background modeling, we can expect to positively explain the γ -ray excess emission from the direction of Tuc-II.

Since the excess obtained from Tuc-II location is below the *Fermi*-LAT's detection level, by using Eq. (4), we have then calculated the possible upper-limit of the pair-annihilation $\langle \sigma v \rangle$ of the WIMPs in Tuc-II, as the function of WIMP mass for five annihilation channels. This method assumes that the entire γ -ray emission arises for particle interaction in that channel only. Additionally, for estimating the uncertainties in J-factor, we have used a Monte Carlo code. The limiting values of J-factor are determined from Eq. (5), with the inputs being the values of the variables (i.e. σ_v , d and R_h) along with their respective uncertainties.

In this paper, we have used larger periods of data compared to the other studies which have analyzed Tuc-II previously [33, 45–47] and this larger dataset have the potential to impose a more stringent constraint on the beyond Standard Model. From our work, we find that even with a median value of the J-factor determined from an approximate, analytical expression given earlier in the literature, our results constraint the blue points in both mSUGRA and MSSM model and uncertainty band have already started to constraint the red models. Due to large uncertainty band in J factor of Tuc-II, maybe it is not possible to notice the significant improvement of constraints on DM models but our result gives a hint that by having a more detailed knowledge of internal structure, Tuc-II has a possibility to impose a very strong constraint on DM models in future. From our analysis results, we have shown that at above 100 GeV DM mass, the $\langle \sigma v \rangle$ upper limit obtained from Tuc-II is comparable with the result obtained from Ret-II. In future, with larger periods of data and with a more precise observation of the internal structure of Tuc-II, we should reduce its J-factor uncertainty band to a possible single upper limit curve of $\langle \sigma v \rangle$ and then Tuc-II might appear as one of the strongest DM dominated UFDs.

A comparative study of the upper limits of WIMP pair-annihilation $\langle \sigma v \rangle$, as obtained in this paper, with the $\langle \sigma v \rangle$ obtained from other studies of the dSphs/UFDs is displayed in Fig. 9. It includes the results obtained from a combined analysis [103] of 15 dSphs from six years of *Fermi*-LAT data, the results from an analysis [104] of γ -ray data from Segue-I, obtained earlier by using the Major Atmospheric Gamma-ray Imaging Cherenkov Telescopes (MAGIC) alone, as well as, the ones obtained from Segue-I by a joint *Fermi*+MAGIC [104] collaboration. Fig. 9 also includes the results from the analysis [105] of data from a combined study of 5 dSphs by the High Energy

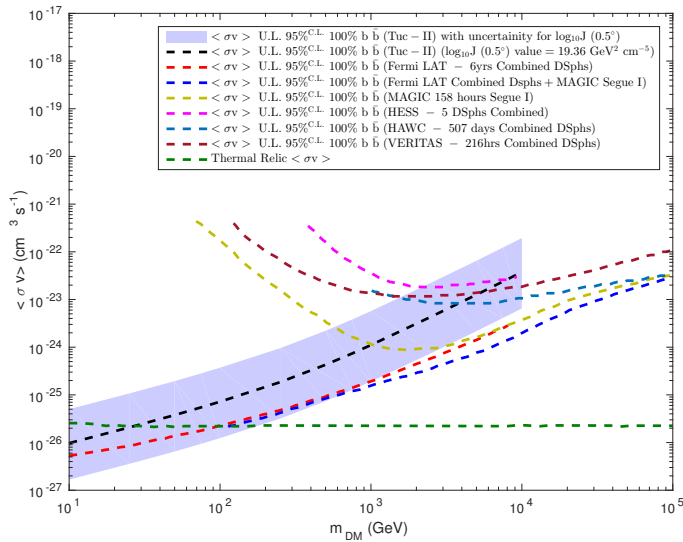


FIG. 9: $\langle \sigma v \rangle$ vs. m_{DM} for $b\bar{b}$ annihilation channel from Tuc-II (obtained in this paper) is shown in comparison with the results obtained from single or combined dSph studies by HESS ([105]), HAWC ([106]), VERITAS ([107]), MAGIC ([104]), *Fermi*-LAT ([103]) and *Fermi*-LAT+MAGIC ([104]) collaboration, respectively. The shaded band represents the uncertainty in the DM density profiles in the Tuc-II. The horizontal dashed sky line corresponds to the relic abundance (or thermal) cross section estimated by Steigman et. al. [89].

Stereoscopic System (H.E.S.S.) of IACT telescopes and the results from the combined study of 15 dSphs [106] by the High Altitude Water Cherenkov (HAWC) gamma-ray observatory and of 4 dSphs [107] by the Very Energetic Radiation Imaging Telescope Array System (VERITAS), as well. In Fig. 9, we find that the joint *Fermi*+MAGIC observations of Segue-I put the best overall limit on the DM annihilation $\langle \sigma v \rangle$ for a wide range of WIMP masses than the limits obtained by various other observations incorporated in that figure. As expected, the combined dSph analysis by the *Fermi*-LAT collaboration also fairs well at masses up to about 1 TeV, above which the *Fermi*-LAT begins to suffer from low statistics. The comparison displayed in Fig. 9 seems to conform to the intuitive belief that the Cherenkov detector arrays should impose stringent limits on the annihilation $\langle \sigma v \rangle$ in the mass range $\gtrsim 10$ TeV, while a joint analysis of spaced-based + ground-based detector is likely to impose the most stringent limits on $\langle \sigma v \rangle$ in the mass range $\lesssim 1$ TeV. It might be interesting to note that the upper-limits on $\langle \sigma v \rangle$ obtained by HAWC and by the *Fermi*+MAGIC collaboration tend to converge in the mass range ≈ 100 TeV, which might indicate that both the IACTs and the Water Cherenkov detectors are becoming competitive in regards to the DM search in the dSphs/UFDs. However, the limiting $\langle \sigma v \rangle$, displayed in Fig. 9, at $\lesssim 1$ TeV WIMP mass range is still about two orders of magnitude away from its relic abundance value. A coordinated effort to combine the data taken from several γ -ray telescopes, as well as, the enhancements of the sensitivity of the Cherenkov telescopes and the improvements of the data analysis techniques of the γ -ray telescopes in general seem, therefore, to be the pressing necessities.

Acknowledgement

We are thankful to the anonymous referee for mentioning some important points which help us to improve our paper a lot. PB is grateful to DST INSPIRE Fellowship Scheme for providing the support for her research. PB would like to thank Dr. Chowdhury Aminul Islam and Prateek Chawla for their valuable discussion. We would like to thank Dr. Stefano Profumo and Dr. Tesla Jeltema of University of California, Santa Cruz, U.S.A., for providing useful guidance in *Fermi*-LAT data analysis. We are particularly grateful to the *Fermi* Science Tools for allowing us to freely access the *Fermi*-LAT data and providing all the needed guidance for our analysis.

-
- [1] E. Komatsu *et al.*, *Astrophys. J. Suppl.* **192**, 18 (2011).
[2] P. A. R. Ade *et al.* [Planck Collaboration], *Astron. and Astrophys.* **594**, A13 (2016).
[3] J. Diemand *et al.*, *Nature*, **454**, 735 (2008).

- [4] V. Springel *et al.*, Mon. Not. R. Astron. Soc., **391**, 1685 (2008).
- [5] A. A. Abdo *et al.*, *Astrophys. J.* **712**, 147 (2010).
- [6] G. Steigman and M. S. Turner, *Nucl. Phys. B* **253**, 375 (1985); G. Bertone, D. Hooper and J. Silk, *Phys. Rept.* **405**, 279 (2005).
- [7] G. Jungman, M. Kamionkowski and K. Griest, *Phys. Rep.* **267**, 195 (1996).
- [8] A. W. McConnachie, *Astron. J.* **144**, 4 (2012).
- [9] S. Piatek *et al.*, *Astrophys. J.*, **124**, 3198 (2002).
- [10] E. K. Grebel *et al.*, *Astron. J.* **125**, 4 (2003).
- [11] N. W. Evans *et al.*, *Phys. Rev. D* **69**, 123501 (2004).
- [12] V. Bonnivard *et al.* *Mon. Not. R. Astron. Soc.*, **453**, 849 (2015).
- [13] D. G. York *et al.*, *Astron. J.* **120**, 1579 (2000).
- [14] V. Belokurov *et al.*, *Astrophys. J.* **712**, L103 (2010).
- [15] N. Kaiser *et al.*, Conference on Survey and Other Telescope Technologies and Discoveries, Waikoloa, Hawaii, August 27-28, (2002), *Proc. SPIE. Int. Soc. Opt. Eng.* **4836**, 154 (2002).
- [16] B. P. M. Laeverts *et al.*, *Astrophys. J.* **813**, 44 (2015).
- [17] B. P. M. Laeverts *et al.*, *Astrophys. J. Lett.* **802**, L18 (2015).
- [18] T. Abbott *et al.* [Dark Energy Survey], arXiv: 0510346v1 (2005).
- [19] K. Bechtol *et al.* [Dark Energy Survey], *Astrophys. J.* **807**, 50 (2015).
- [20] S. E. Koposov *et al.*, *Astrophys. J.* **805**, 130 (2015).
- [21] D. Kim and H. Jerjen, *Astrophys. J. Lett.* **808**, L39 (2015).
- [22] D. Kim *et al.*, *Astrophys. J. Lett.* **804**, L44 (2015).
- [23] N. F. Martin *et al.*, *Astrophys. J. Lett.* **804**, L5 (2015).
- [24] A. Koch *et al.*, *E. Phys. J. web of conferences* **19**, 03002 (2012).
- [25] M. Kuhlen, *2010*, 162083 (2010.).
- [26] A. Drlica-Wagner, Searching For Dwarf Spheroidal Galaxies and Other Galactic Dark Matter Substructure with the Fermi Large Area Telescope, *Ph.D Thesis*, Stanford University, 2013.
- [27] J. D. Simon & M. Geha, *Astrophys. J.* **670**, 313 (2007).
- [28] E. N. Kirby *et al.*, *Astrophys. J.* **779**, 102 (2013).
- [29] A. Frebel, *Astrophys. J. Lett.* **722**, L104 (2010).
- [30] V. Belokurov, *New Astron. Rev.* **57**, 100 (2013).
- [31] T. K. Starkenburg & A. Helmi, *Astron. and Astrophys.* **575**, A59 (2015).
- [32] D. Kim, Search for Ultra-Faint Milky Way Satellites, *Ph.D Thesis*, Australian National University, 2017.
- [33] A. Albert *et al.*, *Astrophys. J.* **834**, 110 (2017).
- [34] M. Ackermann *et. al.* [The Fermi-LAT Collaboration], *Phys. Rev. Lett.* **107**, 241302 (2011).
- [35] M. Ackermann *et. al.* [The Fermi-LAT Collaboration], *Phys. Rev. D* **89**, 04200 (2014).
- [36] M. Ackermann *et al.*, *Phys. Rev. Lett.* **115**, 231301 (2015).
- [37] C. He *et al.*, *Phys. Rev. D* **91**, 063515 (2015).
- [38] A. Drlica-Wagner *et al.* (DES-collaboration), *Astrophys. J.* **813**, 109 (2015).
- [39] M. G. Walker *et al.*, *Astrophys. J.* **819**, 53 (2016).
- [40] G. Gilmore *et al.*, *Nucl. Phys. B* **173**, 15 (2007)
- [41] M. L. Mateo, *Astron. and Astrophys.* **36**, 435 (1998); J. S. Gallagher *et al.*, *Astrophys. J.* **588**, 326 (2003); J. Grcevich and M. E. Putman, *Astrophys. J.* **696**, 385 (2009).
- [42] A. P. Ji *et al.*, *Astrophys. J. Lett.* **832**, L3 (2016).
- [43] N. F. Martin *et al.*, *Astrophys. J.* **684**, 1075 (2008).
- [44] R. R. Munoz *et al.*, *Astron. J.* **140**, 138 (2010).
- [45] D. Hooper & T. Linden, *J. Cosmol. Astropart. Phys.* **09**, 016 (2015).
- [46] F. Calore *et al.*, arXiv:1803.05508v2 (2018).
- [47] A. Drlica-Wagner *et al.* [The DES Collaboration], *Astrophys. J. Lett.* **809**, L4 (2015).
- [48] J. D. Simon *et. al.*, *Astrophys. J.* **808**, 95 (2015).
- [49] M. G. Walker *et al.*, *Astrophys. J.* **808**, 108 (2015).
- [50] S. E. Koposov *et al.*, *Astrophys. J.* **811**, 62 (2015).
- [51] A. Geringer-Sameth *et. al.*, *Phys. Rev. Lett.* **115**, 081101 (2015).
- [52] S. Li *et. al.*, *Phys. Rev. D* **97**, 122001 (2018).
- [53] Y. Zhao, *et. al.*, *Chin.Phys. C* **42**, 025102 (2018).
- [54] T. E. Jeltema and S. Profuma, *J. Cosmol. Astropart. Phys.* **11**, 003 (2008).
- [55] A. Chiti *et. al.*, *Astrophys. J.* **862**, 1 (2018).
- [56] N. W. Evans, J. L. Sanders, A. Geringer-Sameth, *Phys. Rev. D* **93**, 103512 (2016).
- [57] M. G. Walker *et al.*, *Astrophys. J.* **704**, 1274 (2009).
- [58] J. Wolf *et al.* *Mon. Not. R. Astron. Soc.*, **406**, 1220 (2010).
- [59] W. Cash, *Astrophys. J.* **228**, 939 (1979).
- [60] J. R. Mattox, *et al.*, *Astrophys. J.* **461**, 396 (1996).
- [61] F. Acero, *et al.*, *Astrophys. J. Suppl.* **218**, 23 (2015).
- [62] R. Essig, *et al.*, *Phys. Rev. D* **80**, 023506 (2009).
- [63] W. Rolke, A. Lopez, J. Conrad, *Nucl. Instrum. Methods A*, **551**, 493 (2005).

- [64] R. Barbieri, S. Ferrara and C. A. Savay, Phys. Lett. B **119**, 343 (1982).
- [65] O. Helene, Nucl. Instrum. Methods Phys. Res. A, **300**, 132 (1991).
- [66] S. Biswas *et al.* J. Cosmol. Astropart. Phys. **11**, 003 (2017).
- [67] E. A. Baltz *et al.*, J. Cosmol. Astropart. Phys. **07**, 13 (2008).
- [68] J. F. Navarro, C. S. Frenk, S. D. M. White, Astrophys. J. **490**, 493 (1997).
- [69] A.B. Pace *et. al.*, Mon. Not. R. Astron. Soc., **442**, 1718 (2014).
- [70] A. Geringer-Sameth, S.M. Koushiappas and M. Walker, Astrophys. J. **801**, 74 (2015).
- [71] A. B. Pace & L. E. Strigari, arXiv:1802.06811v1 (2018).
- [72] P. Gondolo *et al.*, J. Cosmo Astropart. Phys. **07**, 008 (2004).
- [73] T. Sjostrand, S. Mrenna, P.Z. Skands, Comput. Phys. Commun. **178**, 852 (2008).
- [74] E. Carlson, D. Hooper and T. Linden, Phys. Rev. D. **91**, 061302 (2015).
- [75] M. Ackermann *et al.*, Astrophys. J. **755**, 164 (2012).
- [76] T. Linden, Phys. Rev. D **96**, 083001 (2017).
- [77] Y. Inoue, Astrophys. J. **733**, 66 (2011).
- [78] A. A. Abdo *et al.* (Fermi-LAT Collaboration), Astrophys. J. **720**, 435 (2010).
- [79] D. Hooper *et al.*, Phys. Rev. D **88**, 083009 (2013).
- [80] M. Ackermann et al. (Fermi-LAT Collaboration), Phys. Rev. D **85**, 083007 (2012).
- [81] K. N. Abazajian, S. Blanchet, and J. P. Harding, Phys. Rev. D **84**, 103007 (2011).
- [82] T. M. Venters, Astrophys. J. **710**, 1530 (2010).
- [83] T. M. Venters and V. Pavlidou, Astrophys. J. **737**, 80 (2011).
- [84] A. Cuoco, E. Komatsu, and J. Siegal-Gaskins, Phys. Rev. D **86**, 063004 (2012).
- [85] J. P. Harding and K. N. Abazajian, J. Cosmol. Astropart. Phys. **11**, 026 (2012) .
- [86] E. Massaro *et al.*, Astron. Astrophys. **495**, 691 (2008).
- [87] S. E. Healey *et al.*, Astrophys. J. Suppl. Ser. **171**, 61 (2007).
- [88] A. Geringer-Sameth *et. al.*, arXiv:1807.08740v1 (2018).
- [89] G. Steigman *et. al.*, Phys. Rev. D, **86**, 023506 (2012).
- [90] A. H. Chamseddine, R. Arnowitt, P. Nath, Phys. Rev. Lett. **49**, 970 (1982).
- [91] D. J. H. Chung *et al.*, Phys. Rep. **407**, 1 (2005).
- [92] G. F. Giudice, R. Rattazi, M. A. Luty and H. Murayama, J. High Energy Phys. **12**, 027 (1998); L. Randall and R. Sundrum, Nucl. Phys. B **557**, 79 (1999).
- [93] H. C. Cheng, J. L. Feng, K. T. Matchev, Phys. Rev. Lett. **89**, 211301 (2002).
- [94] G. Servant and T. M. P. Tait, Nucl. Phys. B **650**, 391 (2003).
- [95] D. Hooper and S. Profumo, Phys. Rep. **453**, 29 (2007).
- [96] A. Geringer-Sameth *et. al.*, Phys. Rev. D **91**, 083535 (2015).
- [97] C. Gordon & O. Macias, Phys. Rev. D **88**, 083521 (2013).
- [98] D. Hooper & T. R. Slatyer, Phys. Dark Univ. **2**, 118 (2013).
- [99] T. Daylan *et al.*, Phys. Dark Univ. **12**, 1 (2016).
- [100] B. Zhou *et al.*, Phys. Rev. D **91**, 123010 (2015).
- [101] F. Calore *et al.*, J. Cosmol. Astropart. Phys. **1503**, 038 (2015).
- [102] E. Charles *et al.*, Phys. Rep. **636**, 1 (2016).
- [103] [Fermi-LAT Collaboration] M. Ackerman *et al.*, Phys. Rev. Lett. **115**, 231301 (2015).
- [104] [MAGIC Collaboration] M. L. Ahnen *et al.*, J. Cosmol. Astropart. Phys. **2**, 039 (2016).
- [105] [HESS Collaboration] A. Abramowski *et al.*, Phys. Rev. D **90**, 112012 (2014).
- [106] [HAWC Collaboration] M. L. Proper *et al.*, ICRC, **LA-UR-15-25701**, 0402 (2015).
- [107] [VERITAS Collaboration] S. Archambaut *et al.*, Phys. Rev. D **95**, 082001 (2017).